Chapter 1

Numerical Testing

We have derived two analytic formulae for the effective slip length of a mixed slip surface, using two different mathematical techniques. The homogenized effective slip length is exact in the limit of vanishing period, and is expected to be a useful approximation if a physical system is 'near the limit'. A way to quantify 'nearness to the limit' is to compare the magnitudes of the relevant length scales of the system: the period L of the surface patterning, and the domain height P. Thus, a physical system is near the limit if:

$$L \ll P \tag{1.1}$$

Our perturbative effective slip lengths were also derived with the assumption that $L \ll P$; furthermore, the $b_{\text{eff}} = \langle b \rangle$ expression is expected to be a good approximation when $b \ll L$.

We wish to test our predictions against the 'true' slip lengths of physical systems as they get closer and closer to the relevant limits. Ideally, one would measure effective slip lengths in physical experiments. Such experiments are beyond the scope of this thesis. However, the next best thing are numerical simulations carried out by a computer. Therefore, in this chapter we compare our predicted b_{eff} expressions with effective slip lengths derived from numerical simulations.

1.1 Finite Element Modelling

Perhaps the most powerful and versatile numerical method for solving partial differential equations is Finite Element Modelling (FEM). Many industrial-strength implementations are available; we chose the free and open-source package **FreeFem++**, available from `www.freefem.org` [**?**].

The input to FEM software is a precise description of the model, including the size and shape of the domain, and the equations that hold on the domain and its boundaries. The output of an FEM simulation is a velocity field on the domain.

In our FEM simulations, we used a model with Laplace's equation holding on a rectangular domain of height P, with a fixed shear rate $\dot{\gamma}$ at the top of the domain, periodic boundary conditions on the sides of the domain, and the full tensor slip boundary condition at the bottom of the domain. See Figure (1.1).

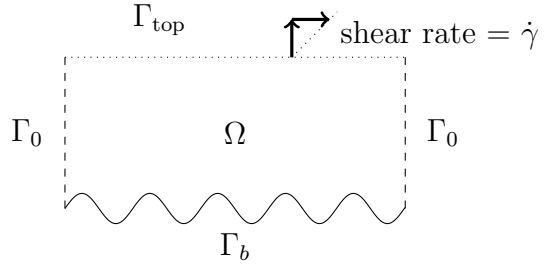

Figure 1.1: Domain Ω with rough slip boundary Γ_b, top boundary Γ_{top} and periodic side boundaries Γ_0.

For convenience when working with slip boundary conditions, in this thesis we adopted the convention that the unit normal vector $\vec{n}$ on the surface points 'up' into the fluid, that is, *into* the domain. This means that the normal vector $\vec{n}$ on the top boundary points *down.*

The flow is shear-driven only. The top fixed-shear boundary condition can be expressed in terms of the deformation rate tensor:

$$2\mathbf{E}(\vec{u}) \cdot \vec{n} = (-\dot{\gamma}, 0) \tag{1.2}$$

(The negative sign is due to the downward-pointing $\vec{n}$ on the top boundary.)

Then the derivation of Section 6.2.3 (page 126) can be augmented with the top shear boundary condition to get:

$$\int_{\Gamma_b} \frac{1}{b}\vec{u}\cdot\vec{g} + \int_{\Gamma_{\text{top}}} (-\dot{\gamma}, 0)\cdot\vec{g} = 2\int_\Omega \mathbf{E}(\vec{u}) : \mathbf{E}(\vec{g}) + \frac{1}{\mu}\int_\Omega \nabla p\cdot\vec{g} \tag{1.3}$$

However, the flow is shear-driven only, with no pressure drop across the domain, so the integral containing the pressure gradient vanishes, leaving:

$$\int_{\Gamma_b} \frac{1}{b}\vec{u}\cdot\vec{g} - \int_{\Gamma_{\text{top}}} (\dot{\gamma}, 0)\cdot\vec{g} = 2\int_\Omega \mathbf{E}(\vec{u}) : \mathbf{E}(\vec{g}) \tag{1.4}$$

Note that the viscosity has vanished due to the periodicity of the pressure.

While our convention of an inward-pointing normal vector $\vec{n}$ was appropriate for studying slip, an *outward-pointing* unit normal is the more common convention in mathematics, including in finite element modelling. To use this last formula in Freefem++, we must change to the outward-pointing convention; this amounts to multiplying b and $\dot{\gamma}$ by -1. Thus, the variational formula used for the Freefem++ simulations was:

$$2\int_\Omega \mathbf{E}(\vec{u}) : \mathbf{E}(\vec{g}) - \int_{\Gamma_{\text{top}}} (\dot{\gamma}, 0)\cdot\vec{g} + \int_{\Gamma_b} \frac{1}{b}\vec{u}\cdot\vec{g} = 0 \tag{1.5}$$

The shear rate $\dot{\gamma}$ was set to one.

Several simulations were done, with different period lengths, on both sinusoidal and flat slip boundaries. An FEM simulation has a mesh defined on the domain, specifying the points at which a velocity solution is found. An adaptive mesh was used, so that each full sine cycle always had at least six mesh points on it, even for very short period lengths.

The mesh and corresponding velocity streamline plot for a couple of simulations are shown in Figure (1.2). Notably, within a period length or two of the sinusoidal surface, the velocity has become uniform horizontal flow.

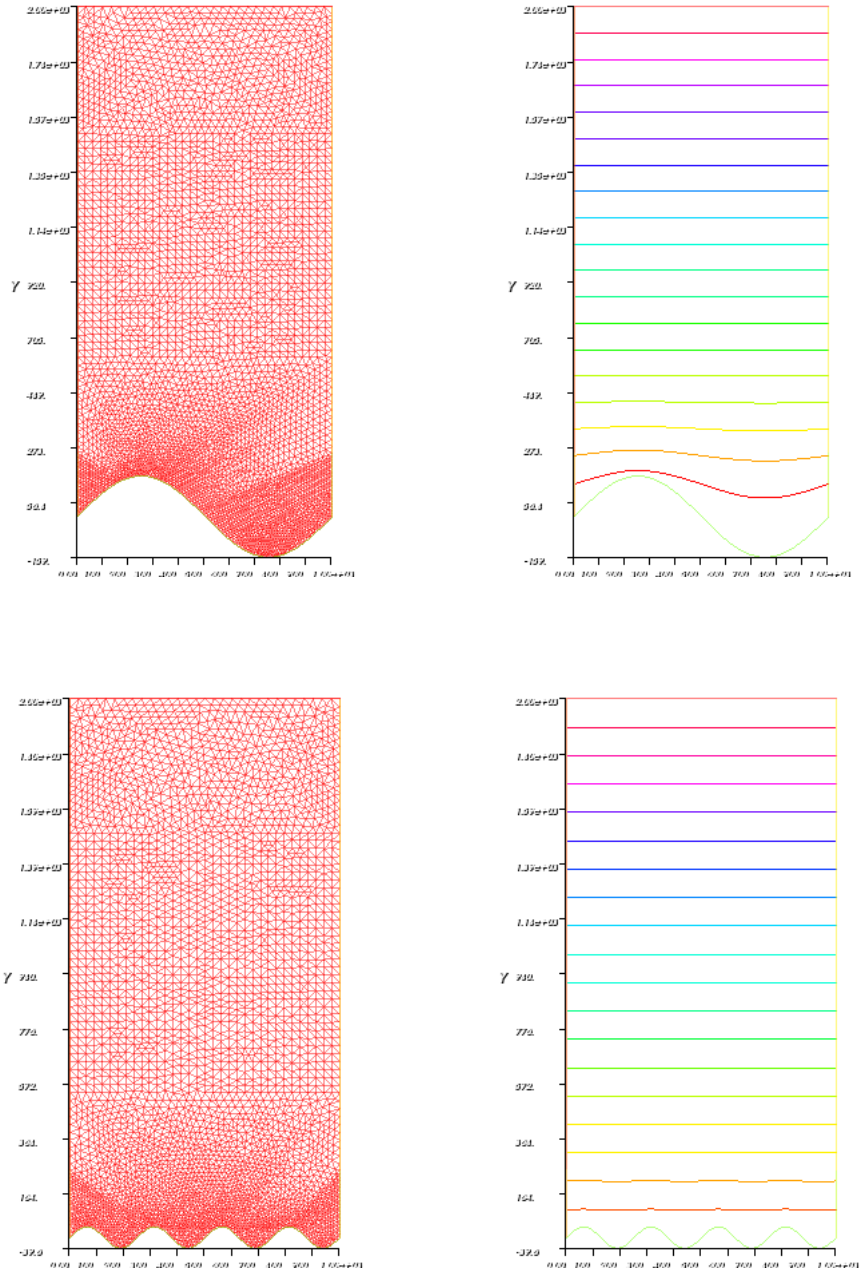

Figure 1.2: The mesh (left) and velocity streamline plot (right) for FEM simulations on a domain with a rough slip surface with one period (top) and four periods (bottom).

The top of the domain, at height P above the slip surface, is known as the far field. The velocity and shear rate in the far field, together with the height, define an effective slip length, as described in Chapter 1. We shall denote this FEM far-field effective slip length as b_{far}. In **all of our simulations**, the far-field velocity turned out to be constant and in the x direction only, even when the period was as large $\frac{1}{2}$ of the domain height. Therefore, b_{far} was always a well-defined single value.

1.1.1 Flat Surface

We start with the simplest case of a flat surface, with a binary slip patterning consisting of alternating stripes of high slip ($b_{\max}$) and low slip ($b_{\min}$) material. The stripes are of equal width; two stripe widths equal the period L.

Harmonic Mean Formula

The homogenization analysis yielded $b_{\text{eff}} = \left\langle \sqrt{1+|\nabla h|^2}/b \right\rangle^{-1}$, which is expected to be a good approximation in the limit $L \ll P, b$. The perturbation analysis yielded $b_{\text{eff}} = \left\langle \frac{1}{b} \right\rangle^{-1}$ – the same formula simplified for flat surfaces. Therefore, we set $b_{\max} = P$ and $b_{\min} = \frac{1}{5}P$, and ran a series of FEM simulations for different values of L, starting with $L = \frac{1}{2}P$, going down to $L = \frac{1}{320}P$. The far-field FEM effective slip length b_{far} was calculated for each simulation. The results are plotted in Figure (1.3).

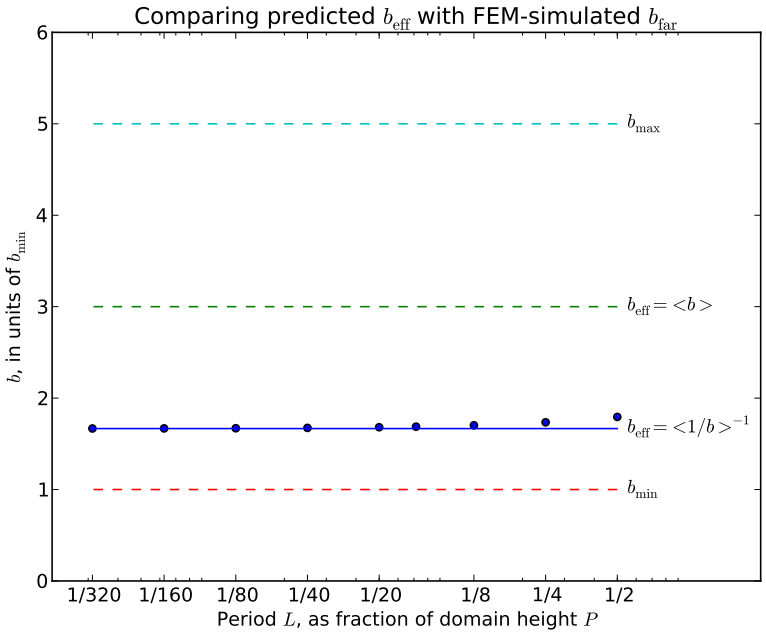

Figure 1.3: Comparison of numerical b_{far} values with predicted b_{eff} for different period sizes, with $b \sim P$. The dots are values of b_{far}. The solid line is the $b_{\text{eff}} = \left\langle \frac{1}{b} \right\rangle^{-1}$ prediction.

As Figure (1.3) shows, if $b \sim P$, the harmonic mean $b_{\text{eff}} = \left\langle \frac{1}{b} \right\rangle^{-1}$ formula is an excellent approximation of b_{far} if $L \ll P$, and still a good approximation even if $L \sim P$. Thus, at least in this numerical simulation, the requirement $L \ll P$ is in practice met by the condition $L \leq \frac{1}{10}P$.

Simple Mean Formula

The perturbation analysis also yielded a formula $b_{\text{eff}} = \langle b \rangle$ in the limit of vanishing slip length. This simple area-weighted mean was derived assuming $L \ll P$, and is expected to be a good approximation to b_{far} in the limit $b \ll L \ll P$. To explore this, we ran a series of FEM simulations with fixed $L = \frac{1}{10}P$, and $b_{\max}$ varying from $b_{\max} = P$ down to $b_{\max} = \frac{1}{400}P$. The b_{far} of each simulation is plotted as a dot in Figure (1.4).

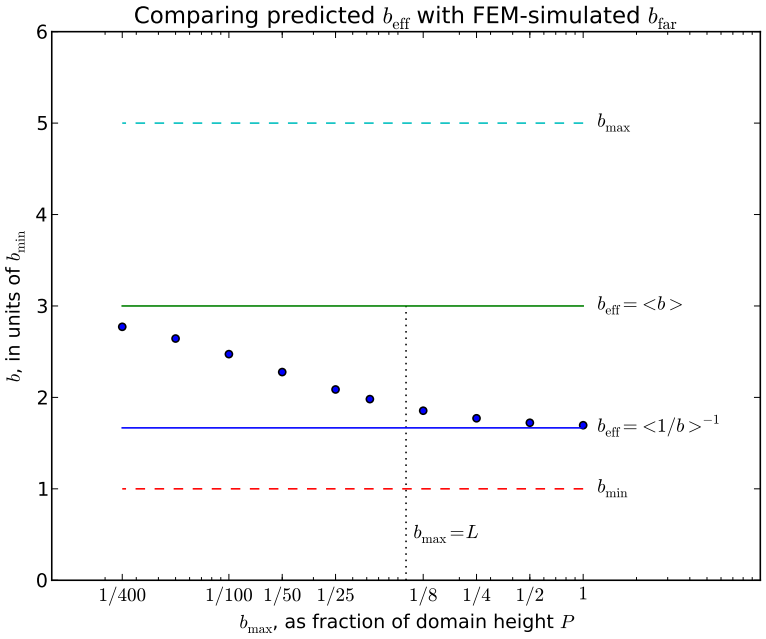

Figure 1.4: Comparison of numerical b_{far} values with b_{eff} predictions, for different values of $b_{\max}$, with $L = \frac{1}{10}P$. The dots are values of b_{far}. The lower solid line is the $b_{\text{eff}} = \left\langle \frac{1}{b} \right\rangle^{-1}$ prediction, and the upper solid line is $b_{\text{eff}} = \langle b \rangle$ prediction. The vertical dotted line indicates where $b_{\max} = L$.

The values of b_{far} in Figure (1.4) demonstrate a gradual transition from the regime where $b_{\text{eff}} = \left\langle \frac{1}{b} \right\rangle^{-1}$ applies to the regime where $b_{\text{eff}} = \langle b \rangle$ applies. Figure (1.4) affirms that $b_{\text{eff}} = \left\langle \frac{1}{b} \right\rangle^{-1}$ is an excellent approximation in the regime $L \ll b, P$, and reveals that $b_{\text{eff}} = \left\langle \frac{1}{b} \right\rangle^{-1}$ is a surprisingly good ap-

proximation in the regime $L \sim b \ll P$. The 'limit of vanishing slip length' is shown to be quite a strong condition: The regime $b \approx \frac{1}{10}L \ll P$ is a 'transition regime', with the b_{far} values midway between the simple mean and the harmonic mean; the simple mean is not a good approximation until $b_{\max} \leq \frac{1}{40}L$.

1.1.2 Rough Surface

The FEM testing on a flat surface showed our harmonic mean $b_{\text{eff}} = \left\langle \frac{1}{b} \right\rangle^{-1}$ formula to be an excellent approximation in the regime $L \ll P, b_{\max}$. We now wish to investigate the importance of the arc-length correction – the correction due to the increased area of liquid-solid contact on a rough surface.

To that end, we ran a series of FEM simulations with sinusoidal surfaces. Each surface was a corrugation with the standard sine-wave profile – the amplitude and period are always in the ratio $1 : 2\pi$. The slip length varied in a binary fashion, with high slip in the valleys of the sinusoid, and low slip on the peaks of the sinusoid. This models a nanograting with air pockets in the grooves. The flow was shear-driven by a fixed shear rate, and the slip lengths were fixed at $b_{\min} = \frac{1}{5}P$, $b_{\max} = P$. A schematic appears in Figure (1.5).

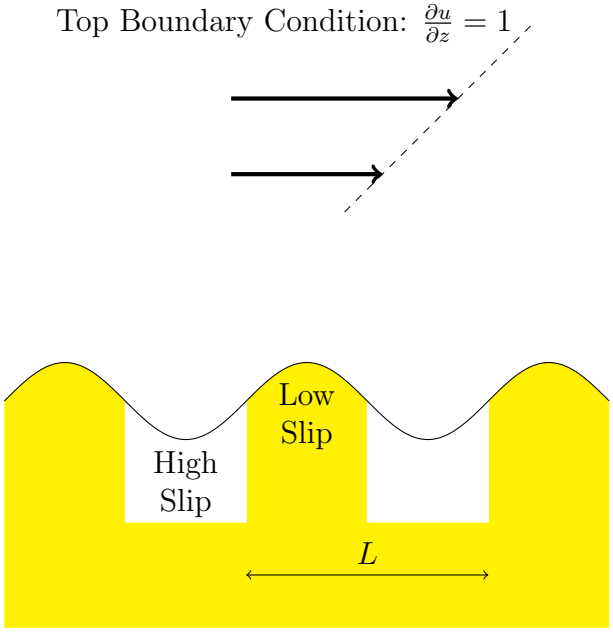

Figure 1.5: Schematic of the FEM model with corrugated mixed-slip surface.

A series of FEM simulations were done with different periods of the sinusoidal corrugation, starting from $L = \frac{1}{2}P$, down to $L = \frac{1}{200}P$. The b_{far} from

each simulation appears as a dot in the plot of Figure (1.6).

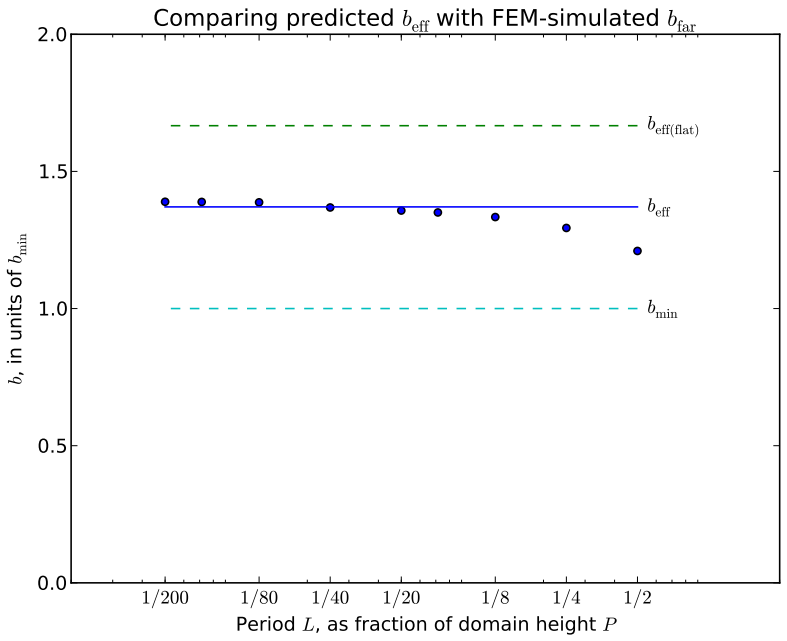

Figure 1.6: Comparison of numerical b_{far} values with b_{eff} predictions for **sinusoidal** surfaces for different periods, with $b \sim P$. The dots are values of b_{far}. The solid line is the $b_{\text{eff}} = \left\langle \sqrt{1+|\nabla h|^2}/b \right\rangle^{-1}$ prediction. The upper dashed line is the $b_{\text{eff(flat)}} = \left\langle \frac{1}{b} \right\rangle^{-1}$ predicted if the surface were assumed to be flat.

Figure (1.6) clearly shows the significance of the arc length correction: The full $b_{\text{eff}} = \left\langle \sqrt{1+|\nabla h|^2}/b \right\rangle^{-1}$ expression with arc length correction is shown as the solid line, and the b_{far} values converge on this line as L gets smaller. The $b_{\text{eff(flat)}} = \left\langle \frac{1}{b} \right\rangle^{-1}$ calculated if the surface were assumed to be flat is shown as the upper dotted line. Thus, if $b \sim P$, then the full b_{eff} prediction is an excellent approximation when $L \ll P$.

To better test the accuracy of the b_{eff} prediction, we calculated the differences between the b_{far} values and b_{eff}, expressed as a percentage of b_{eff}. The resulting percentage differences are plotted in Figure (1.7).

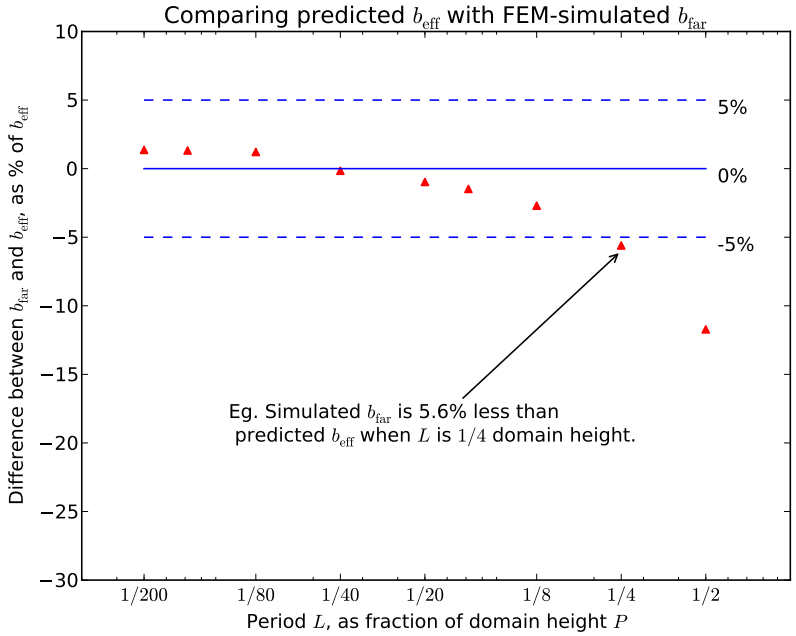

Figure 1.7: Percentage comparisons between numerical b_{far} values and contact-area-corrected $b_{\text{eff}} = \left\langle \sqrt{1+|\nabla h|^2}/b \right\rangle^{-1}$ predictions. The dots are values of b_{far}, expressed as the percentage $(b_{\text{far}} - b_{\text{eff}})/b_{\text{eff}} \times 100$.

The percentage differences of Figure (1.7) reveal that our contact-area-corrected $b_{\text{eff}} = \left\langle \sqrt{1+|\nabla h|^2}/b \right\rangle^{-1}$ prediction for rough surfaces is accurate to within a few % when $L \ll P, b_{\text{max}}$. For example: Accurate to within 5% when $L \leq \frac{1}{5}P$, and within 1% when L is less than 5% of P.

The slip lengths in these FEM simulations were calculated with respect to the $z = 0$ line, about which the sinusoids oscillate. In Chapter 3 we noted the ambiguity in the definition of slip length – does the surface begin at the $z = 0$ line or at the tops of the sine wave peaks? To investigate this issue, we recalculated the measured slip lengths with respect to the **tops of the peaks**. These are plotted as the crosses in Figure (1.8) (along with the 'uncorrected' slip lengths).

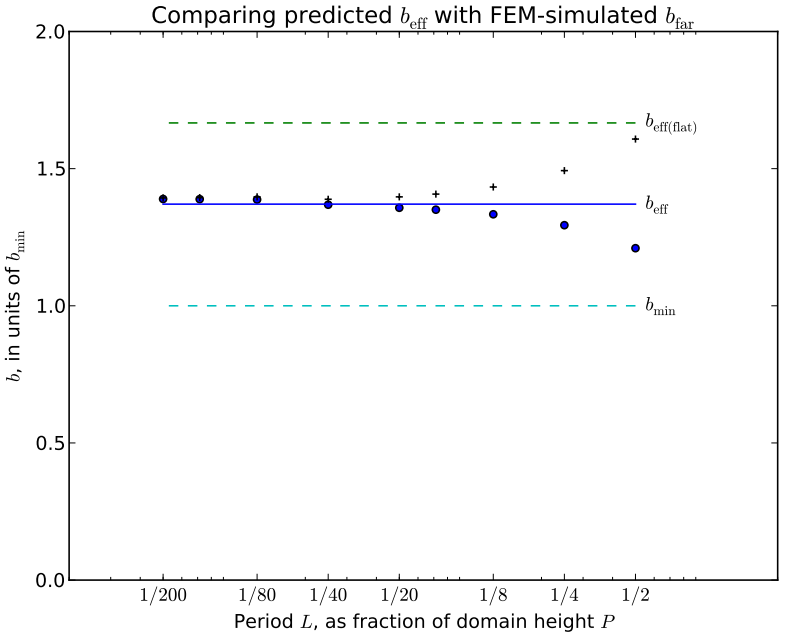

Figure 1.8: Comparison of numerical b_{far} values with b_{eff} predictions for **sinusoidal** surfaces for different periods, with $b \sim P$. The dots are values of b_{far} calculated w.r.t. the $z = 0$ line, and the crosses are b_{far} values calculated w.r.t. the top of the sinusoid. The solid line is the $b_{\text{eff}} = \left\langle \sqrt{1 + |\nabla h|^2}/b \right\rangle^{-1}$ prediction. The upper dashed line is the $b_{\text{eff(flat)}} = \left\langle \frac{1}{b} \right\rangle^{-1}$ predicted if the surface were assumed to be flat.

Figure (1.8) shows that the slip lengths defined with respect to the tops of the surface peaks differ from the predicted b_{eff} by about the same amount as the $z = 0$ based slip lengths – but in the other direction. In other words, for a given period L, the predicted b_{eff} value lies between the two numerical b_{far} values calculated with respect to the two different reference points. The difference between the two types of b_{far} values increases as L increases, because the roughness amplitude increases in concert. The accuracy of b_{eff} depends on how the measured b_{far} values are calculated, and the 'correct' way to calculate b_{far} depends on the circumstance. If effective slip lengths are measured with respect to the tops of the roughness, then our b_{eff} predic-

tions will underestimate measured effective slip lengths.

A final note about numerical issues: A close look look at the data plotted in Figure (1.7) reveals that the numerics and the prediction agree better and better as L gets smaller and smaller — up to a point. Then the prediction *underestimates* the numerical values. We believe this to be a computational artefact, due to an insufficient number of lattice points on a very rapidly oscillating boundary: When we noticed that the b_{far} values overshot the prediction, we ran the same simulations with double the number of lattice points. The overshoot reduced, so we further increased the number of lattice points, which gave even better results. At some point we hit the limit of our computational power, but it is reasonable to think that given sufficient computational power, the discrepancy would disappear.

1.2 Finite Difference Numerics

As an exercise, the same slip problem was also solved numerically using the finite difference method. The main benefit of this exercise (apart from educational) was that the software employed allowed the easy visualisation of 3-dimensional flow fields. We employed Python using the Numpy library, which is a front end to various very fast C and Fortran libraries, and the Mayavi library for visualisation. A curved boundary is difficult to implement in this approach, so the case of the flat slip boundary was studied.

Three-dimensional velocity profiles were generated. The x-velocity u for flow over a mixed-slip surface is shown in Figure (1.9).

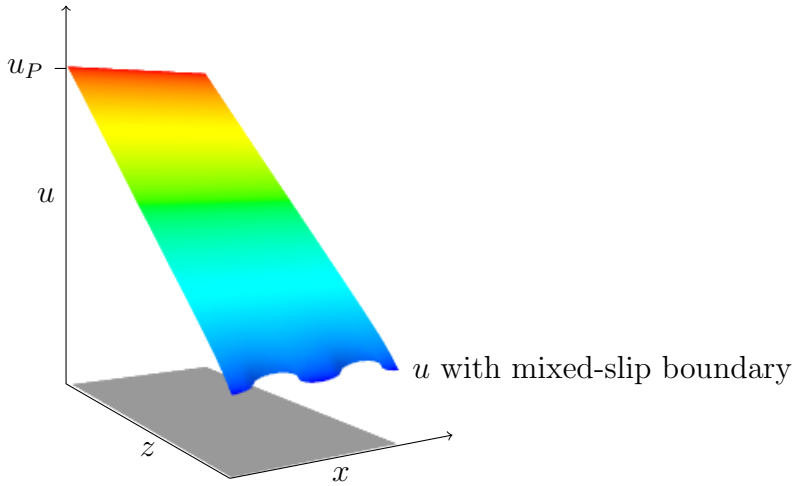

Figure 1.9: The coloured surface is u, the x-velocity component of a velocity field of a finite difference simulation of flow over a flat mixed-slip surface.

The x-velocity is high and uniform at the top boundary condition (large z), and varies periodically over the slip boundary.

To provide some perspective, flow profiles over *pure* high-slip and low-slip surfaces were generated. These are plotted together, along with the mixed-slip flow profile, in Figure (1.10).

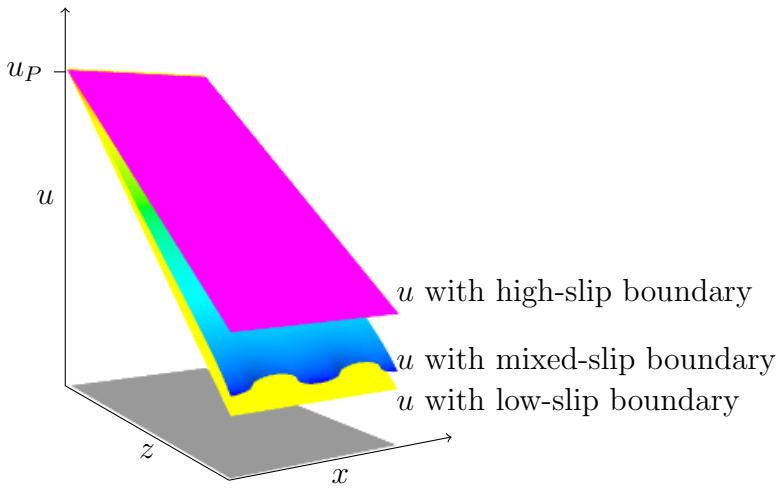

Figure 1.10: The same mixed-slip flow field as in Figure (1.9), plus the flow solutions for flow over the purely high-slip surface (pink), and the purely low-slip surface (yellow).

There is an interesting feature in the mixed-slip flow field: while the velocity at the slip boundary varies periodically, the variation is not very large. The slip velocity does *not* swing between the extremes of velocities over the pure high-slip and low-slip surfaces. Instead, the slip velocity has only a moderate periodic variation about a central value.

What is that central value? Of course, we expect it to be the slip velocity that would occur if the surface had a single slip length equal to our predicted b_{eff}. We explore this by generating a last flow profile with a pure b_{eff} slip length surface. We plot this (in black) together with the mixed-slip flow profile in Figure (1.11).

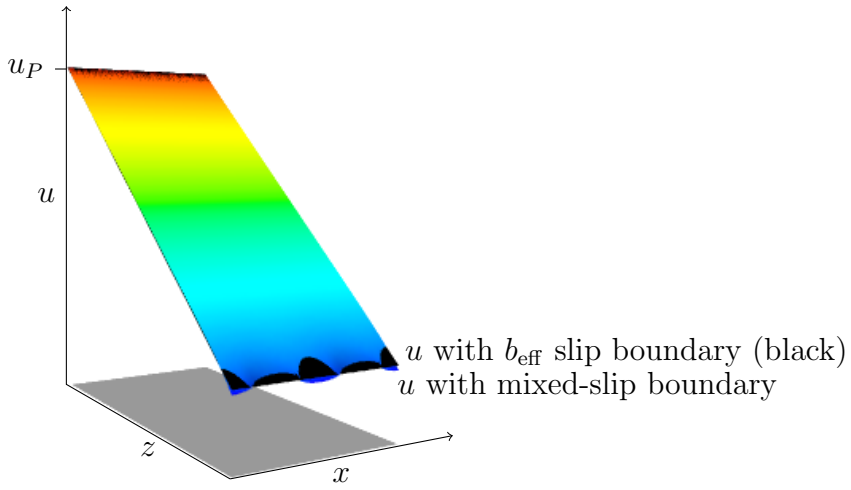

Figure 1.11: The same mixed-slip flow field as in Figure (1.9), plus the flow field corresponding to a homogeneous boundary of slip length b_{eff} (black).

Figure (1.11) shows excellent agreement between the effective flow profile and the mixed-slip profile. For most of the domain, they are almost indistinguishable. Only very close to the slip boundary does the mixed-slip profile exhibit a periodic variation about the effective slip profile.

The plot of Figure (1.11) also throws light on another issue: how thick is the boundary layer? The boundary layer can be arbitrarily defined to end where the flow becomes (arbitrarily close to) uniform. Without being quantitative, we can see that a reasonable choice for boundary layer thickness d could be less than the period L.

1.3 Conclusion

Numerical simulations reveal that if the period of surface patterning L is much less than the domain height P and typical slip lengths, then the effective slip length as defined in the far field of the system is very well approximated by:

$$b_{\text{eff}} = \left\langle \frac{\sqrt{1+|\nabla h|^2}}{b} \right\rangle^{-1} \tag{1.6}$$

The b_{eff} expression incorporates a correction for the increased area of solid-liquid contact in rough surfaces. Numerical testing shows this correction to be accurate, so therefore our b_{eff} expression of Equation (1.6) is valid for both flat and rough surfaces.

Numerical simulations further reveal that if $L \ll P$ and slip lengths are of the same order as the period, $L \sim b$, then Equation (1.6) is a surprisingly good approximation for effective slip lengths.

If slip lengths are much smaller than any other length scale, then the effective slip length is best approximated by a simple area-weighted mean. Numerical testing with a flat surface showed that if $b_{\max} \leq \frac{1}{40} \ll P$, then the effective slip length is well approximated by:

$$b_{\text{eff}} = \langle b \rangle \tag{1.7}$$